Received: 15 March 2018 | Revised: 13 September 2018 | Accepted: 2 October 2018

DOI: 10.1002/hbm.24418

WILEY

RESEARCH ARTICLE

Directed functional connections underlying spontaneous brain activity

Ana Coito[1,2] | Christoph M. Michel[1] | Serge Vulliemoz[2†] | Gijs Plomp[3†]

[1]Functional Brain Mapping Laboratory, Department of Fundamental Neurosciences, Faculty of Medicine, University of Geneva, Geneva, Switzerland

[2]Epilepsy Unit, University Hospital of Geneva, Geneva, Switzerland

[3]Perceptual Networks Group, Department of Psychology, University of Fribourg, Fribourg, Switzerland

Correspondence
Serge Vulliemoz, Epilepsy Unit, University Hospital of Geneva, Rue Gabrielle-Perret-Gentil 4, 1211, Geneva, Switzerland.
Email: serge.vulliemoz@hcuge.ch

Funding information
Foundation Gertrude von Meissner; Swiss National Science Foundation, Grant/Award Numbers: CRSII5_170873, 320030-169198, 320030_159705, PP00P1_157420

Abstract

Neuroimaging studies have shown that spontaneous brain activity is characterized as changing networks of coherent activity across multiple brain areas. However, the directionality of functional interactions between the most active regions in our brain at rest remains poorly understood. Here, we examined, at the whole-brain scale, the main drivers and directionality of interactions that underlie spontaneous human brain activity by applying directed functional connectivity analysis to electroencephalography (EEG) source signals. We found that the main drivers of electrophysiological activity were the posterior cingulate cortex (PCC), the medial temporal lobes (MTL), and the anterior cingulate cortex (ACC). Among those regions, the PCC was the strongest driver and had both the highest integration and segregation importance, followed by the MTL regions. The driving role of the PCC and MTL resulted in an effective directed interaction directed from posterior toward anterior brain regions. Our results strongly suggest that the PCC and MTL structures are the main drivers of electrophysiological spontaneous activity throughout the brain and suggest that EEG-based directed functional connectivity analysis is a promising tool to better understand the dynamics of spontaneous brain activity in healthy subjects and in various brain disorders.

KEYWORDS

default-mode network, electroencephalography, granger causality, graph theory, resting-state

1 | INTRODUCTION

In the last two decades, functional magnetic resonance imaging (fMRI) has shown that spontaneous brain activity is characterized by coherent and correlated fluctuations of activity in specific sets of brain areas (Biswal, Yetkin, Haughton, & Hyde, 1995; Damoiseaux et al., 2006; Raichle et al., 2001). The areas showing increased and correlated activations at rest are known as resting-state networks (RSN) and correspond spatially to networks associated with specific tasks (somato-motor, visual, cognitive, etc). Functional RSN patterns are correlated with structural connectivity patterns (Honey et al., 2009). One particular RSN is the default-mode network (DMN), which has the highest activity in resting wakefulness and includes the posterior cingulate cortex (PCC), the medial prefrontal cortex, the medial temporal regions, and the inferior parietal cortex (Buckner, Andrews-Hanna, & Schacter, 2008; Greicius, Krasnow, Reiss, & Menon, 2003; Greicius, Supekar, Menon, & Dougherty, 2009). Although RSNs were initially studied with techniques that assume stationarity across time, we now know that these networks are highly dynamic (de Pasquale, Corbetta, Betti, & Della Penna, 2017), their predominance alternates in time (Chang & Glover, 2010; Zalesky, Fornito, Cocchi, Gollo, & Breakspear, 2014) and RSNs can overlap both in spatial layout and in temporal dynamics (Karahanoglu & Van De Ville, 2015).

Better knowledge about the main drivers of spontaneous brain activity and the directionality of interactions is crucial to better understand the core organization of spontaneous brain activity and how it differs in neurological disorders. Several fMRI studies have investigated directional influences among DMN nodes using both Granger causality and dynamic causal modeling (DCM), but inconsistent results have been found (Deshpande, Santhanam, & Hu, 2011; Di & Biswal, 2014; Jiao et al., 2011; Li, Wang, Yao, Hu, & Friston, 2012; Razi, Kahan, Rees, & Friston, 2015; Uddin, Kelly, Biswal, Castellanos, &

[†]These authors contributed equally to this work.

Milham, 2009; Yan & He, 2011; Zhou et al., 2011). EEG and magnetoencephalography (MEG) could be key to gain important additional insights into whole brain resting-state directed functional connectivity, because they provide a more direct measure of neuronal activity than fMRI, and have a much higher temporal resolution (Lopes da Silva, 2013). RSNs have individual complex electrophysiological signatures (Brookes, Hale, et al., 2011a; de Pasquale et al., 2010; Laufs et al., 2003; Mantini, Perrucci, Del Gratta, Romani, & Corbetta, 2007) and networks obtained from MEG and EEG recordings were shown to be similar to the fMRI RSNs (Britz, Van De Ville, & Michel, 2010; Brookes, Woolrich, et al., 2011b; Chen, Ros, & Gruzelier, 2013; Liu, Farahibozorg, Porcaro, Wenderoth, & Mantini, 2017; Maldjian, Davenport, & Whitlow, 2014). These studies, however, looked at spatial correlations with EEG and not at the temporal properties of these networks. Moreover, they used seed-based correlation or independent component analysis that could not inform about the directions of information transfer in spontaneous activity.

Here, we combined EEG and multivariate Granger causality analysis (Astolfi et al., 2006; Baccala & Sameshima, 2001; Plomp, Quairiaux, Michel, & Astolfi, 2014) to investigate which brain regions consistently influence activity in other regions. Granger causality is a directed functional connectivity measure based on the relative predictability of recorded signals (Bressler & Seth, 2011; Granger, 1969) that has been formally validated in epicranial EEG recordings from rats [Plomp et al., 2014]. Directed functional connectivity analyses based on Granger causality have previously been used to study sensory processing using EEG (Astolfi et al., 2007; Plomp, Hervais-Adelman, Astolfi, & Michel, 2015) and MEG (Michalareas et al., 2016), and the pathological spread of activity in epilepsy (Coito et al., 2015; Ding, Worrell, Lagerlund, & He, 2007).

To address which regions are the major drivers of ongoing large-scale spontaneous activity dynamics, we applied Granger causality analysis to high-density EEG source signals recorded from 35 healthy subjects at rest, followed by graph analysis to study network properties. The results shed light on which brain regions drive resting brain activity, and could potentially lead to better biomarkers of brain disorders.

2 | METHODS

2.1 | Subjects, high-density EEG recording and preprocessing

Thirty five healthy subjects (mean subject age 30 ± 9 years-old, 18 women) underwent a 10–15 min of resting-state eyes-closed high-density EEG recording (256 electrodes, *Electrical Geodesics Inc., Eugene, OR*) while instructed to remain awake. Their wakefulness was confirmed a posteriori during EEG inspection. We removed the facial and neck electrodes as those are usually contaminated with muscle artifacts, ending up with 204 electrodes for analysis. All subjects were right handed except one. Impedances were kept as low as possible for all the electrodes (<30 kΩ). The sampling frequency of all recordings was 1,000 Hz and data sets were downsampled offline to 250 Hz. All signals were filtered between 1 and 100 Hz using a Butterworth non-causal filter.

Because the signal-to-noise ratio (SNR) of spontaneous EEG is limited on the single epoch level, we sampled randomly in the whole recording 60 nonoverlapping artifact-free epochs of 1 s from each subject, thus focusing our analysis on directed interactions that are present across mental states. We visually inspected each epoch's EEG signals and voltage topographies for bad channels, which were interpolated using the three-dimensional (3D) splines method, and made sure that the analyzed epochs were free of eye movement, muscle, or other artifacts.

2.2 | Electrical source imaging and selection of regions of interest

Electric source imaging (ESI) applied to high-density EEG recordings is a clinically validated technique to estimate neuroelectrical activity of cortical regions (Brodbeck et al., 2011; Darvas, Pantazis, Kucukaltun-Yildirim, & Leahy, 2004; Megevand et al., 2014; Michel et al., 2004; Rikir et al., 2014). Here, we applied ESI to reconstruct the source activity that underlay the maps of scalp potentials. We computed individual forward models using a simplified realistic head model with consideration of scalp, skull, and brain thicknesses (locally spherical model with anatomical constraints, LSMAC [Brunet, Murray, & Michel, 2011]). A 3D grid of equally distributed solution points (between 3,000 and 5,000) was placed in the gray matter, obtained from the segmented individual T1-weighted MRI ($1 \times 1 \times 1$ mm^3). We used a linear distributed inverse solution with biophysical constraints (local auto-regressive averages, LAURA [Grave de Peralta Menendez, Murray, Michel, Martuzzi, & Gonzalez Andino, 2004]) to calculate the 3D current source density. The current source density was computed for each time point of each epoch.

For each subject, the gray matter was parceled in 82 regions of interest (ROIs) using the automated anatomical labeling (AAL) digital atlas (Tzourio-Mazoyer et al., 2002) coregistered with the inverse segmentation matrix obtained in SPM8 (www.fil.ion.ucl.ac.uk/spm). The full list of all 82 regions can be found in the Supporting Information. The solution point closest to the centroid of each ROI was considered to represent the source activity of the ROI. The 3D orientation of the source dipoles was taken into account, by projecting them on the predominant dipole direction of each ROI across time and epochs (Coito et al., 2015; Plomp, Leeuwen, & Ioannides, 2010).

Given that connectivity algorithms take scalar time-series as their input, and as ESI outputs 3D time-series (amplitudes in the *x*, *y*, and *z* direction), we then determined the predominant dipole orientation for each epoch and projected the *x*, *y*, and *z* time-series onto this dipole to obtain a scalar time-series, in the same way that we have previously described (Coito, Michel, van Mierlo, Vulliemoz, & Plomp, 2016; Sperdin et al., 2018). Following previous work, we first computed an average dipole direction considering only the 10% strongest norms of the dipoles across time and epochs. Second, we flipped the sign of all dipoles whose direction was negative with respect to the average direction. Final, each 3D dipole was projected onto this flipped direction to obtain a scalar value, using the dot product of the

XYZ coordinates of each dipole to the XYZ coordinates of the positive-signed direction (Coito, Michel, et al., 2016).

EEG and ESI analysis were carried out using the freely available software *Cartool* (https://sites.google.com/site/cartoolcommunity/) and custom-made Matlab scripts.

2.3 | Power spectral density and weighted partial directed coherence

For each subject and epoch, we computed the spectral power of the source signals at each ROI. To get an accurate frequency representation and avoid the problem of frequency doubling when the fast Fourier transform (FFT) is computed in the source activity domain, we first computed the FFT for each scalp electrode. We then computed the ESI in the real and imaginary part of the FFT separately and then combined them, obtaining the spectral power at each source point, for each epoch (Koenig & Pascual-Marqui, 2009; Yuan, Doud, Gururajan, & He, 2008). The mean spectral power for each patient was computed and normalized (0–1) across regions, time and frequencies (1–40 Hz) by subtracting the minimum power and dividing by the range.

To investigate the directionality of functional brain connections, Granger-causality (Granger, 1969), can be reliably applied to electrophysiological signals in a data-driven approach (Lopes da Silva, 2013). To estimate the directed functional connections between source regions, we used a variant of the partial directed coherence (PDC), a multivariate Granger-causality approach in the frequency domain (Astolfi et al., 2006; Baccala & Sameshima, 2001; Granger, 1969; Plomp et al., 2014) named weighted partial directed coherence (wPDC) (Coito, Michel, et al., 2016; Plomp et al., 2014). This multivariate analysis refers to the simultaneous investigation of the pairwise directed relationships between all signals. Granger-causal modeling using EEG relies on the temporal precedence between signals and has been well-validated, showing reliable and informative connectivity patterns obtained from electrophysiological recordings (Bastos et al., 2015; Bressler & Seth, 2011; Brovelli et al., 2004; Michalareas et al., 2016; Plomp et al., 2014; Saalmann, Pinsk, Wang, Li, & Kastner, 2012). Using human EEG recordings, we have previously estimated directed functional connectivity of cortical sources in patients with temporal lobe epilepsy and found connectivity alterations concordant with cognitive deficits during transient epileptic activity as well as striking network alterations even in the absence of detectable epileptic activity (Coito et al., 2015; Coito, Genetti, et al., 2016a). PDC is derived from multivariate autoregressive models (MVAR) that are fit to the data with an appropriate model order. Here, we used a model order of 10, corresponding to 40 ms of the signal, in line with our previous work (Coito, Genetti, et al., 2016a). PDC values were scaled (in the same way as the spectral power) and multiplied by the spectral power of the source region (weighted PDC, wPDC [Plomp et al., 2014]):

$$\mathrm{wPDC}_{ij}(f) = \frac{|A_{ij}(f)|^2}{\sum_{m=1}^{K} |A_{im}(f)|^2} \cdot \mathrm{SP}_j(f) \quad (1)$$

where j is the source region, i is the sink region, K is the number of regions, SP_j is the spectral power of the source region j and $A_{\mathrm{ROIs}\times\mathrm{ROIs}}(f)$ is the ROIs × ROIs matrix of MVAR model coefficients transformed to the frequency domain. These coefficients were estimated using the Nutall-Strand algorithm (Marple, 1987; Schlögl, 2006). According to (Blinowska, 2011), the number of data points should be higher than the number of parameters: $K*N > K*K*p$, where: K is the number of regions, N is the number of data points and p is the model order). Here, we obtain 82*(250*60) > 82*82*10, or 18 times more data points than parameters. The normalization of the MVAR coefficients in (1) is done at each discrete time point and independent of the model order used. The MVAR coefficients at each time point reflect processes that go back 10 steps.

For each subject, we obtained a four-dimensional asymmetrical connectivity matrix (ROIs × ROIs × frequency × epochs), which represents the flow from one ROI to another in a certain frequency and for each epoch. We then averaged this matrix across epochs. Averaging of single trial wPDC is similar to the approach used in (Ghumare, Schrooten, Vandenberghe, & Dupont, 2015), where the single trial model parameters are averaged. In a recent work, it was shown that such an approach in real data often performs better than the traditional approach of creating one MVAR model of the ensemble of trials (Pagnotta & Plomp, 2018). Connectivity analyses were carried out in *Matlab* (MATLAB and Statistics Toolbox Release 2012b). For some figures, we modified scripts from the e-connectome toolbox (He et al., 2011).

2.4 | Surrogate data generation and statistical analysis

To statistically evaluate the reliability of the connectivity results, we generated a surrogate data set by randomizing the phases of all 82 source signals of each subject and computed then the wPDC in this surrogate data set. We used the phase-randomization surrogate data technique described by Theiler, Eubank, Longtin, Galdrikian, & Doyne Farmer, 1992 (Theiler et al., 1992). In this method, the surrogate data is generated by randomizing the phases of the signal while keeping the amplitude spectra of the original signal. For each original data set, 50 surrogates were generated. wPDC was computed for each surrogate epoch and averaged across epochs. Although scaling with the spectral power could introduce systematic variations in surrogate outflow, we did not find such positive dependency in the generated surrogate data, nor in the real data (Supporting Information Figure S1).

All comparisons between real and surrogate connectivity results were carried out using a nonparametric statistical test (Mann–Whitney–Wilcoxon). To correct for multiple testing, the false discovery rate (FDR) approach was used (Benjamini & Hochberg, 1995) ($p < .05$).

2.5 | Network topology

Directed functional connectivity yields directed and weighted graphs in which each edge value corresponds to the strength of the connection (wPDC). This is therefore a fully connected network with wPDC values as edge weights. We computed the sum of the outflows from each region to all others (the summed outflow) at each frequency bin (Bullmore & Sporns, 2009; Coito et al., 2015). The summed outflow of a source region j (sof_j) at a given frequency f is given by:

$$\mathrm{sof}_j(f) = \sum_i^K \mathrm{wPDC}_{ij}(f) \quad (2)$$

The summed outflow reflects the driving importance of a region in the network (Bullmore & Sporns, 2009; Coito et al., 2015). We refer to the regions with strongest summed outflow as "main drivers", as those are the ones with highest information outflow and therefore driving importance toward other regions. To assess the reliability of the identified main drivers across subjects, we calculated for real and surrogate data the number of subjects whose strongest outflow was from the identified main drivers.

To investigate clusters of interconnected brain regions, and therefore have an insight into functional brain segregation, we computed the clustering coefficient. It represents the number of connections that exist between neighbors of a node as a proportion of all possible connections (Bullmore & Sporns, 2009). To identify the central nodes of the network, that is, nodes crucial for functional integration, and thus, information transfer in the network, we computed the betweenness centrality. It quantifies the number of shortest paths between all node pairs that pass through that node (Bullmore & Sporns, 2009). We computed another measure of functional integration: the efficiency. It is the inverse of the shortest path length, which is the average minimum number of nodes that have to be crossed to go from one node to any other (Bullmore & Sporns, 2009). We computed these measures for each subject's real and surrogate connectivity matrix using the weighted directed functions available in the Brain Connectivity Toolbox (Rubinov & Sporns, 2010). We then statistically compared the groups (Mann–Whitney–Wilcoxon, $p < .05$, FDR correction).

3 | RESULTS

3.1 | PCC is the main driver of spontaneous activity

Inspecting the frequency distribution of total summed outflow, we found a clear peak around 10 Hz (Figure 1a). We therefore restricted the subsequent analyses to the alpha band (7–12 Hz). We identified the regions with statistically significant higher summed outflow in real than in surrogate data (Figure 1b). The regions with highest summed outflow were the bilateral PCC, hippocampus, parahippocampal gyrus, amygdala, anterior cingulate cortex (ACC), and olfactory cortex (all $p < 10^{-10}$, FDR corrected) (Figure 1b). To further assess the reliability of the identified main drivers across subjects, we calculated, for real and surrogate data, the number of subjects whose strongest driver was the PCC (i.e., the strongest driver was either the left or the right PCC), one of the regions of the medial temporal lobe (MTL, i.e., amygdala or hippocampus or parahippocampal gyrus), the ACC (i.e., the strongest driver was either the left or the right ACC), or any of the other 72 regions, using a chi-square test (Figure 2). We found that in 18/35 subjects and 3/35 surrogates, the strongest summed outflow was from the PCC ($p < 10^{-4}$), 12/35 subjects and 1/35 surrogates from the MTL ($p < 10^{-3}$), 2/35 subjects, 14/35 surrogates from the ACC ($p < 10^{-3}$), and 3/35 subjects and 17/35 surrogates from other regions ($p < 10^{-3}$). This confirms on the individual subject level that PCC and MTL areas are the two most important drivers of spontaneous brain activity.

We found that the strongest outflows, among those with statistically significant increases in real versus surrogate data, originated predominantly from the PCC and were directed toward widespread brain areas ($p < 10^{-11}$, FDR corrected, for all PCC outflows) (Figure 3).

The regions with the highest clustering coefficient, betweenness centrality and efficiency, that were significantly different in real versus surrogate data, were bilateral PCC, hippocampus, parahippocampal gyrus, amygdala, and olfactory gyrus (all clustering coefficient and efficiency comparisons showed $p < 10^{-10}$; betweenness centrality showed overall $p < .005$, FDR corrected). The bilateral ACC also had a high clustering coefficient and efficiency that was significantly different in real versus surrogate data (in all, $p < 10^{-10}$, FDR corrected). These areas are illustrated in Figure 1c–e.

3.2 | Directed interactions among the main drivers

Having identified the main driving regions from EEG recordings and the PCC as the major driver, we then asked whether PCC's driving role effectively resulted in a directed interaction patterns from posterior to anterior DMN regions. For this analysis, we selected the 10 strongest drivers, which showed close correspondence to the typical DMN regions (Figure 4), and subtracted backward connections from forward connections and divided by the total summed outflow. We found that 27 of the 35 subjects had stronger net forward connections ($p < .018$, chi-square test; null hypothesis: number of subjects with more forward and with more backward connections is the same) (Figure 4). Using the same approach for interhemispheric connections, we found no evidence for a left–right asymmetry in the directed interactions between these 10 core regions (20 of the 35 subjects had more left to right connections, n.s.).

4 | DISCUSSION

We investigated the directed interactions that underlie spontaneous brain activity using whole-brain directed functional connectivity analysis and network topology based on high-density EEG. From the 82 brain regions analyzed, we identified the PCC, MTL regions (hippocampus, parahippocampal gyrus, amygdala), ACC, and the orbitofrontal cortex (olfactory gyrus) as the main drivers of resting-state activity as well as important nodes accounting for integration, segregation and information transmission in the large-scale brain network. This manifested itself as a high summed outflow from these regions as well as a high betweenness centrality, clustering coefficient, and efficiency. All of these measures were significantly increased in real versus surrogate data sets. Our results suggest that the dynamics of spontaneous brain activity is predominantly driven by the PCC as well as by MTL structures. Furthermore, we found that interactions were directed more strongly from posterior toward anterior than the other way.

4.1 | Main drivers identified from EEG analysis overlap with the default mode network

Using a data-driven EEG-based directed functional connectivity approach, we here show that most of the strongest drivers of

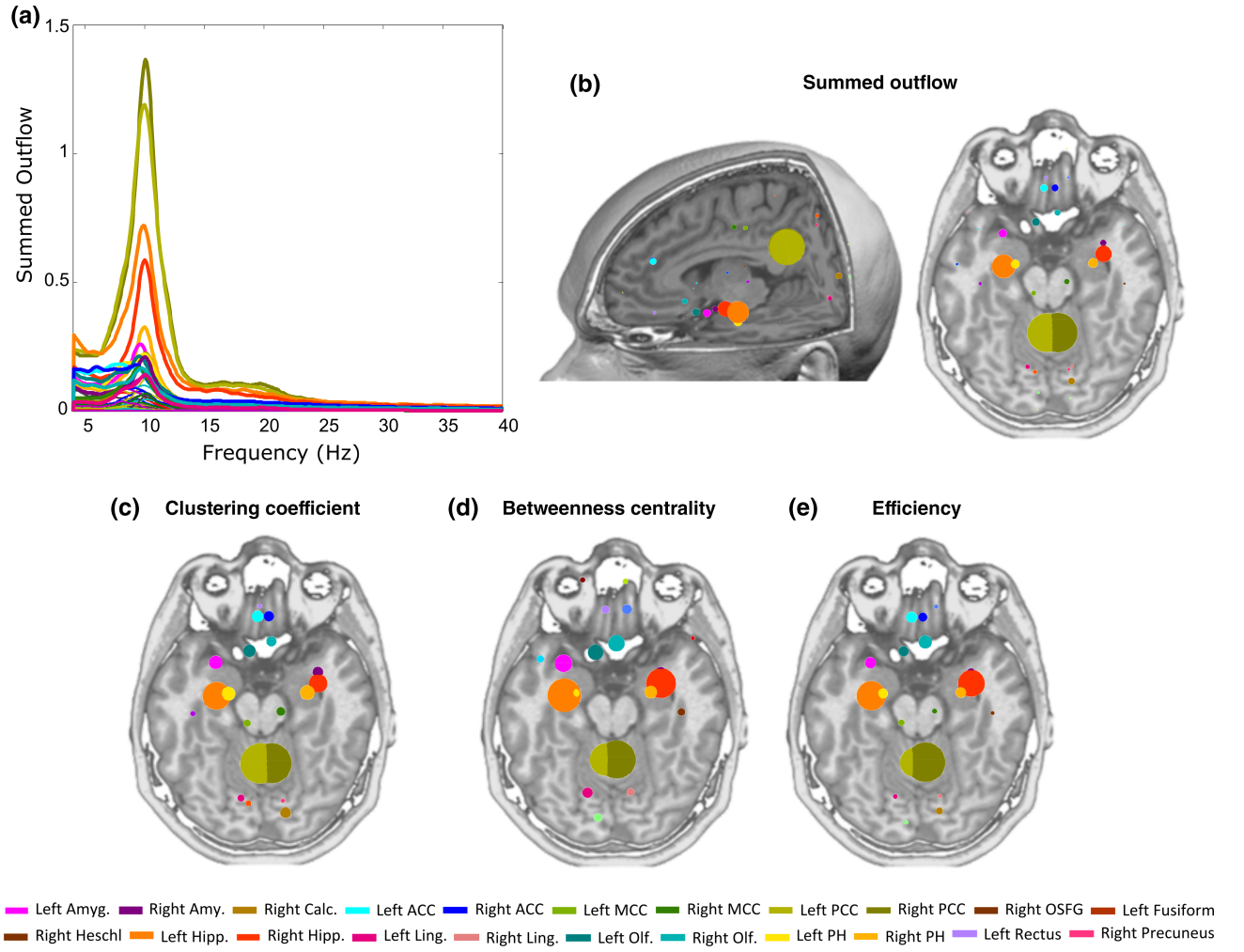

FIGURE 1 Network topology results. (a) Summed outflow across frequencies (4–40 Hz) for all 82 ROIs. (b) Alpha-band statistically significant increases in summed outflow (spheres) relative to surrogate data obtained from phase-shuffling of the original data. The size of the sphere reflects summed outflow. (c) Alpha-band significant clustering coefficient (spheres). (d) Alpha-band significant betweenness centrality (spheres). (e) Alpha-band significant efficiency (spheres). The bigger the sphere, the higher the topology value in that region [Color figure can be viewed at wileyonlinelibrary.com]

electrophysiological activity in the resting brain represented a network concordant with the DMN (PCC and medial temporal lobe regions) consistent with fMRI and DTI studies (Buckner et al., 2008; Greicius et al., 2003; Greicius et al., 2009). These regions are among the most globally connected regions in the brain (Buckner et al., 2009; Cole, Pathak, & Schneider, 2010; Hagmann et al., 2008) and are consistent major functional cortical hubs of spontaneous activity, as evidenced by fMRI (de Pasquale et al., 2017).

RSNs measured using fMRI can be paralleled by EEG or MEG data. Power in the delta, theta, alpha, beta and gamma frequency bands measured with M/EEG has been shown to be correlated with BOLD signals or with the RSNs depicted by fMRI (Brookes, Hale, et al., 2011a; de Pasquale et al., 2010; Laufs et al., 2003; Mantini et al., 2007). In addition, the networks derived from MEG (Brookes, Woolrich, et al., 2011b; Maldjian et al., 2014), low-density EEG data (19 electrodes) (Chen et al., 2013), or high-density EEG (Britz et al., 2010; Liu et al., 2017) were similar to RSNs derived from fMRI.

The PCC's key role in resting-state activity is well-established (de Pasquale et al., 2017; Vogt & Laureys, 2005). The PCC has been consistently found as a functional and structural key region of the DMN (Fransson & Marrelec, 2008; Hagmann et al., 2008; van den Heuvel, Kahn, Goni, & Sporns, 2012; van Oort, Cappellen van Walsum, & Norris, 2014) with connections to the medial temporal and

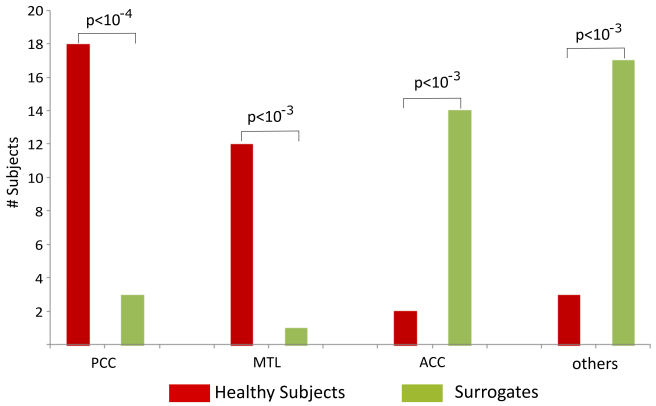

FIGURE 2 Comparison of the number of subjects and surrogate data whose strongest outflow was the PCC, medial temporal lobe regions (MTL, i.e., either amygdala or hippocampus or parahippocampus), ACC, or any of the remaining 72 regions ("other ROIs") [Color figure can be viewed at wileyonlinelibrary.com]

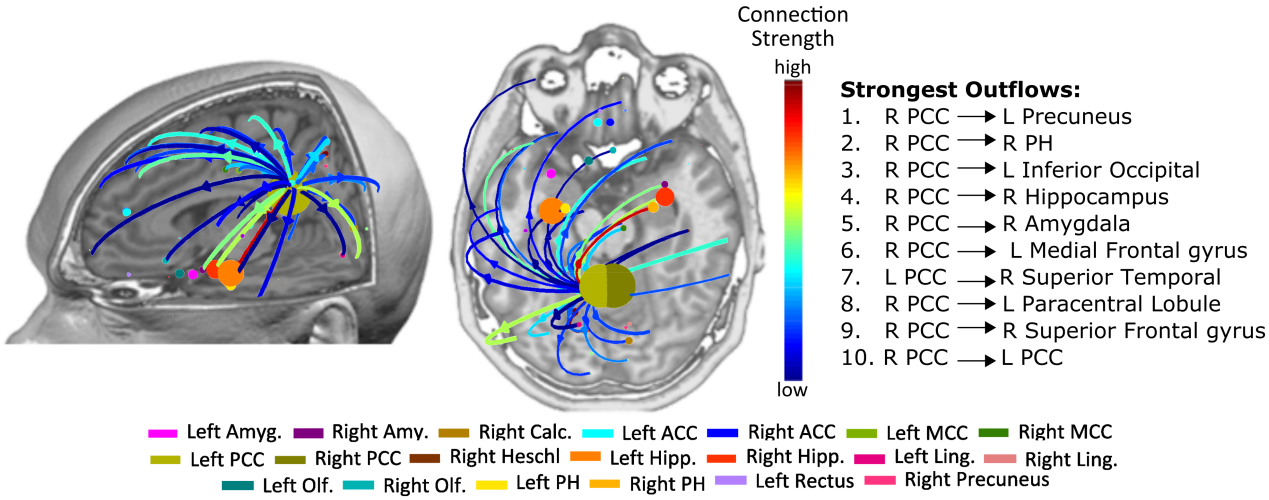

FIGURE 3 Statistically significant outflows (arrows) (only the 0.5% strongest outflows are shown) between real and surrogate data. The right column indicates the top 10 strongest significant outflows [Color figure can be viewed at wileyonlinelibrary.com]

frontal lobes (Buckner et al., 2008; Greicius et al., 2009; Hagmann et al., 2008; van den Heuvel, Mandl, Luigjes, & Hulshoff Pol, 2008). Likewise, regions of the DMN, including the PCC, are densely interconnected by white-matter tracts that form part of the core structural network of the brain (Hagmann et al., 2008). An fMRI study, using also a data-driven approach, observed strong interactions between the PCC and all the other regions of the DMN, suggesting that the PCC is a key structure mediating activity in this network (Fransson & Marrelec, 2008). Other studies have also corroborated this finding, as reviewed in de Pasquale et al. (2017). At rest, the metabolic activity in the PCC was shown to be higher than in other regions in humans (Gusnard & Raichle, 2001). The PCC was also found to have a higher neuronal firing rate at rest than during tasks in macaques (Hayden, Smith, & Platt, 2009), providing further physiological evidence of the importance of the PCC for the resting-state. It is also known from anatomical studies in primates that the PCC is interconnected (sends and receives projections) with MTL regions (parahippocampal regions) and the frontal lobe, namely the mid-dorsolateral prefrontal cortex and ACC (Parvizi, Van Hoesen, Buckwalter, & Damasio, 2006).

Using directed functional connectivity analysis, we here found that the PCC is the strongest driver of spontaneous activity in healthy humans with the strongest connections initiating from this region and directed toward the medial temporal and frontal lobes. Moreover, we showed that the PCC had the highest betweenness centrality and efficiency, corroborating its crucial importance in mediating functional integration, the ability to combine specialized information from distributed brain regions, as shown by previous fMRI and DTI studies (Achard, Salvador, Whitcher, Suckling, & Bullmore, 2006; van Oort et al., 2014). The PCC also had a high clustering coefficient, suggesting that the PCC also plays a role in functional segregation, that is, the ability for specialized processing to occur in densely interconnected clusters of regions (Rubinov & Sporns, 2010). Our results also showed that MTL regions were strong drivers of spontaneous activity, possibly reflecting the noted presence of autobiographical memories in spontaneous thought processes (Christoff, Irving, Fox, Spreng, & Andrews-Hanna, 2016). The fact that the strongest driver in 30 out of 35 subjects was either the PCC or the MTL, compared to only 4 out of 35 surrogates, indicates that our results are highly unlikely to have occurred by chance.

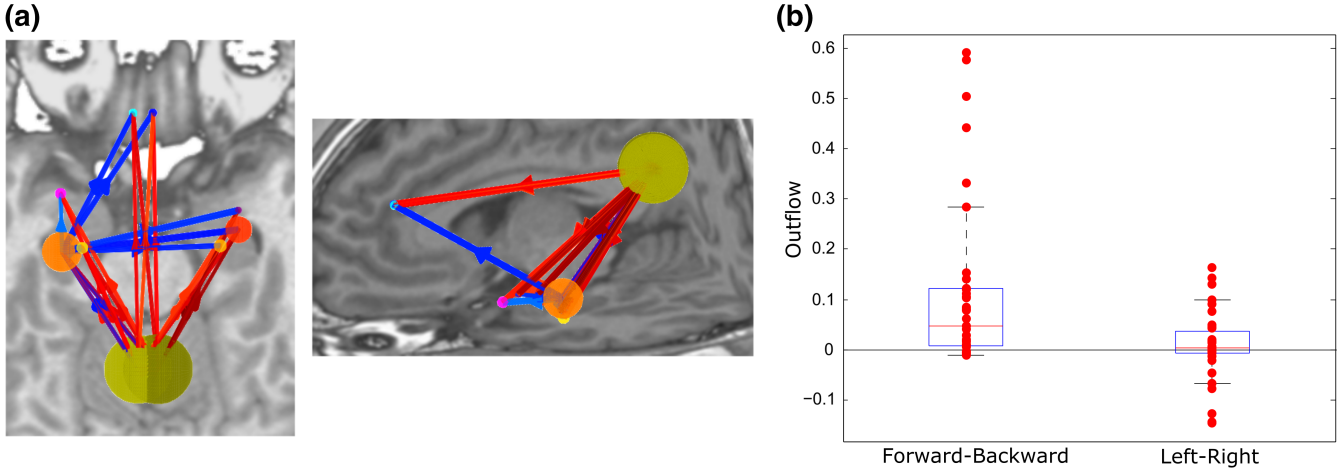

FIGURE 4 (a) Strongest outflows between the default-mode network regions (percentile for showing outflows: 70%). (b) Differences between forward and backward, and left and right outflows [Color figure can be viewed at wileyonlinelibrary.com]

Taken together, our findings suggest that PCC and MTL regions segregate information and relay it forward to more anterior regions (functional integration), resulting in predominant interactions from posterior toward anterior brain areas during spontaneous brain activity. We did not see any evidence of a lateralization of functional connections, which suggests that the global left and right outflows in the DMN seem to be balanced.

Our analysis was carried out in the alpha band because a spectral peak was clearly observed in this frequency band, which is mandatory for the identification of a brain oscillation (Lopes da Silva, 2013). In addition, the peak driving was found in this frequency band. EEG activity in the alpha band represents the hallmark of resting-state brain activity in healthy subjects. Oscillations in the alpha frequency range are considered as optimal to gate information transfer across specific populations (Lopes da Silva, 2013). It is well-accepted that alpha rhythm does not represent an "idling" state of the brain, but plays a pivotal role in attention, perception, cognition, and motor control (Laufs et al., 2003; Pfurtscheller & Lopes da Silva, 1999; Thut, Schyns, & Gross, 2011), so that a large body of brain connectivity studies have focused and reported on interactions in the alpha band.

4.2 | Comparison with fMRI studies

Relatively few fMRI studies have investigated the directional influence among the DMN nodes, using either Granger-causality (Deshpande et al., 2011; Jiao et al., 2011; Uddin et al., 2009; Yan & He, 2011; Zhou et al., 2011) or DCM (Di & Biswal, 2014; Li et al., 2012; Razi et al., 2015). However, there remains considerable inconsistency between studies independently of the technique used. For instance, in Di & Biswal (2014), it was reported that interactions were directed from the medial prefrontal cortex to the PCC, while other studies, reported a causal influence from the PCC toward the medial prefrontal cortex (Li et al., 2012) and (Razi et al., 2015).

Despite large concordance, some spatial differences were noted between our results and fMRI studies regarding the DMN. The inferior parietal cortex has been reported by fMRI studies as being part of the DMN (Buckner et al., 2008; Horn, Ostwald, Reisert, & Blankenburg, 2014), but it was not identified here as one of the most important nodes of the resting-state using EEG-based resting-state connectivity. This could be due to the fact that recordings were performed with eyes closed, and that the parietal cortex is known to be involved in visual attention and directing eye-movements (Corbetta & Shulman, 2002). Previous DCM fMRI studies did not include the MTL, although they have also been shown to be part of the DMN (Buckner et al., 2008; Greicius et al., 2003; Greicius et al., 2009). Our results suggest that MTL structures are also important nodes of the resting brain. The strong outflow from the orbito-frontal cortex (olfactory cortex) in our study could be due to the very close proximity to the medial prefrontal cortex part of the DMN regions found in fMRI studies. The relatively low spatial resolution of ESI in basal frontal areas makes it difficult to confirm this interpretation. Beyond differences related to directed versus undirected measures, it is important to note that the Granger-causal modeling approach used here is a multivariate analysis simultaneously investigating the relationships between all signals, whereas fMRI analysis is most often bivariate. The use of multivariate connectivity methods has been shown to be superior to bivariate measures for assessing causal relationships and directions (Blinowska, 2011; Kus, Kaminski, & Blinowska, 2004). A limitation of multivariate methods is the high dimensionality of model parameters and it has been recommended that the number of data points exceeds the number of parameters by at least a factor of 10 to assure reliable results (Blinowska, 2011). Although our data-parameter ratio of 18 is adequate, we also controlled for spurious findings by using phase-shuffled surrogate data (Lizier, Heinzle, Horstmann, Haynes, & Prokopenko, 2011).

Other functional RSNs have consistently been reported in resting-state fMRI studies, such as the motor network, the visual network, two lateralized networks consisting of the superior parietal and superior frontal regions, and a network consisting of bilateral temporal/insular and ACC regions (Biswal et al., 1995; Damoiseaux et al., 2006; De Luca, Beckmann, De Stefano, Matthews, & Smith, 2006). In our findings, the nodes as well as the connections belonging to these networks were not among the strongest drivers of the resting-state. This could be due to the fact that they have a lower whole-brain outflow, although they may have a high local outflow or inflow to or from certain regions, as well as methodological differences due to the signal origin (electric vs. metabolic). Nevertheless, the same approach could be applied to specifically study directed functional connectivity in predefined sets of regions corresponding to other RSNs.

4.3 | Potential applications to neurological and psychiatric disorders

The investigation of the strength and directionality of interactions in the resting human brain could help to better understand cognitive deficits associated to network disruption in certain neurological disorders, and provide new biomarkers of these disorders. We have previously applied this methodological approach in temporal lobe epilepsy (TLE), to study both interictal spikes (Coito et al., 2015) and resting-state (Coito, Genetti, et al., 2016a). In the latter study, the predominance of the PCC and MTL structures was consistently observed in all groups (left TLE, right TLE, and controls), but the connection strengths were significantly weaker in both TLE groups compared to the healthy subjects group. The resting-state connectivity patterns were also different in patients compared with healthy controls, as the latter showed that the strongest driving occurred from the PCC, while in both TLE groups, the strongest driving was from the hippocampus ipsilateral to the epileptic focus (Coito, Genetti, et al., 2016a). EEG-based connectivity measures appear promising to investigate alterations of directed connectivity in other neurological and psychiatric conditions (Greicius, 2008; Greicius, Srivastava, Reiss, & Menon, 2004).

4.4 | Methodological considerations

From a methodological point of view, there are strong arguments to apply connectivity analysis to ESI sources rather than EEG signals directly from the sensors (electrodes), as it avoids volume conduction and reference problems that hamper the validity of direct analysis of electrode signals (Schoffelen & Gross, 2009; Van de Steen et al., 2016). Several invasive studies support ESI as an accurate sublobar localization technique as validated by intracranial EEG recordings and

epilepsy surgery of epileptic activity and cognitive evoked potentials in the hippocampus (Brodbeck et al., 2011; Megevand et al., 2014; Nahum et al., 2011; Rikir et al., 2014). There is increasing evidence that ESI applied to high-density EEG can estimate cortical activity from deep regions such as the cingulate, medial frontal, orbitofrontal and medial temporal lobe, as shown by simultaneous scalp and intracranial recordings (Koessler et al., 2015; Nahum et al., 2011; Ramantani et al., 2014). However, ESI might have difficulty distinguishing between strictly temporo-polar and medial temporal sources (amygdala, anterior hippocampus) and a clear subdivision between the source activity or connectivity related these two regions remains to be considered with caution.

We here used the approach of averaging over many epochs to obtain the predominant drivers across networks and network changes occurring in spontaneous activity. The relatively low SNR of EEG recordings compared to fMRI limits the possibility of network identification on the single epoch basis, thus preventing windows-based or point-process approaches on continuous signals typically used in fMRI dynamics (Karahanoglu & Van De Ville, 2015). Future directed connectivity work using EEG could use alternative approaches to study the directed connectivity of other RSN (Britz et al., 2010; Vidaurre et al., 2016) and provide a more fine-grained characterization of how changes between specific RSNs come about.

In this study, we analyzed summed outflows to study of the main drivers of spontaneous activity. The wPDC formulation used in this study was therefore optimized for investigating outflows by normalizing the coefficients of the MVAR model by the inflows (Astolfi et al., 2007; Coito, Michel, et al., 2016; Kus et al., 2004; Plomp, et al., 2014). The investigation of the distribution of summed inflows was not in the focus of this study. For a reliable estimation of the inflows, a normalization by the outflows would be needed as in the original definition of PDC (Baccala & Sameshima, 2001).

5 | CONCLUSIONS

Here, we investigated the drivers and directionality of interactions in the resting human brain at a whole-brain scale, using high-density scalp EEG recordings. Our work shows that directed interactions from the PCC and MTL are the main drivers of spontaneous activity dynamics, and showing the highest integration and segregation importance. This suggests an important role for directed interactions from the PCC and MTL in switching between momentarily dominant network states. Furthermore, we showed that the strongest drivers were coincident with the DMN, which demonstrates a good potential for the use of EEG-based measures to study resting-state connectivity. The directional information, coupled to the low-cost of EEG, could strengthen its use in the study of DMN alterations in clinical populations and the potential development of biomarkers.

ACKNOWLEDGMENTS

This study was supported by the Swiss National Science Foundation (SNSF) grants PP00P1_157420, 320030_159705, 320030-169198 and CRSII5_170873, and by the Foundation Gertrude von Meissner. The Cartool software (https://sites.google.com/site/cartoolcommunity/home) has been programmed by Denis Brunet from the Functional Brain Mapping Laboratory, Geneva, and is supported by the Center for Biomedical Imaging of Geneva and Lausanne (CIBM), Switzerland.

CONFLICT OF INTEREST

The authors declare that they do not have any conflict of interest.

ORCID

Ana Coito https://orcid.org/0000-0003-1797-5819

REFERENCES

Achard, S., Salvador, R., Whitcher, B., Suckling, J., & Bullmore, E. (2006). A resilient, low-frequency, small-world human brain functional network with highly connected association cortical hubs. *The Journal of Neuroscience: The Official Journal of the Society for Neuroscience*, *26*, 63–72.

Astolfi, L., Cincotti, F., Mattia, D., Marciani, M. G., Baccala, L. A., de Vico Fallani, F., … Babiloni, F. (2006). Assessing cortical functional connectivity by partial directed coherence: Simulations and application to real data. *IEEE Transactions on Bio-Medical Engineering*, *53*, 1802–1812.

Astolfi, L., Cincotti, F., Mattia, D., Marciani, M. G., Baccala, L. A., de Vico Fallani, F., … Babiloni, F. (2007). Comparison of different cortical connectivity estimators for high-resolution EEG recordings. *Human Brain Mapping*, *28*, 143–157.

Baccala, L. A., & Sameshima, K. (2001). Partial directed coherence: A new concept in neural structure determination. *Biological Cybernetics*, *84*, 463–474.

Bastos, A. M., Vezoli, J., Bosman, C. A., Schoffelen, J. M., Oostenveld, R., Dowdall, J. R., … Fries, P. (2015). Visual areas exert feedforward and feedback influences through distinct frequency channels. *Neuron*, *85*, 390–401.

Biswal, B., Yetkin, F. Z., Haughton, V. M., & Hyde, J. S. (1995). Functional connectivity in the motor cortex of resting human brain using echo-planar MRI. *Magnetic Resonance in Medicine*, *34*, 537–541.

Blinowska, K. J. (2011). Review of the methods of determination of directed connectivity from multichannel data. *Medical & Biological Engineering & Computing*, *49*, 521–529.

Bressler, S. L., & Seth, A. K. (2011). Wiener-granger causality: A well established methodology. *NeuroImage*, *58*, 323–329.

Britz, J., Van De Ville, D., & Michel, C. M. (2010). BOLD correlates of EEG topography reveal rapid resting-state network dynamics. *NeuroImage*, *52*, 1162–1170.

Brodbeck, V., Spinelli, L., Lascano, A. M., Wissmeier, M., Vargas, M. I., Vulliemoz, S., … Seeck, M. (2011). Electroencephalographic source imaging: A prospective study of 152 operated epileptic patients. *Brain: A Journal of Neurology*, *134*, 2887–2897.

Brookes, M. J., Hale, J. R., Zumer, J. M., Stevenson, C. M., Francis, S. T., Barnes, G. R., … Nagarajan, S. S. (2011a). Measuring functional connectivity using MEG: Methodology and comparison with fcMRI. *NeuroImage*, *56*, 1082–1104.

Brookes, M. J., Woolrich, M., Luckhoo, H., Price, D., Hale, J. R., Stephenson, M. C., … Morris, P. G. (2011b). Investigating the electrophysiological basis of resting state networks using magnetoencephalography. *Proceedings of the National Academy of Sciences of the United States of America*, *108*, 16783–16788.

Brovelli, A., Ding, M., Ledberg, A., Chen, Y., Nakamura, R., & Bressler, S. L. (2004). Beta oscillations in a large-scale sensorimotor cortical network: Directional influences revealed by granger causality. *Proceedings of the National Academy of Sciences of the United States of America*, *101*, 9849–9854.

Brunet, D., Murray, M.M., Michel, C.M. (2011) Spatiotemporal analysis of multichannel EEG: CARTOOL. *Computational Intelligence and Neuroscience*, *2011*:813870, 1, 15.

Buckner, R. L., Andrews-Hanna, J. R., & Schacter, D. L. (2008). The brain's default network: Anatomy, function, and relevance to disease. *Annals of the New York Academy of Sciences*, *1124*, 1–38.

Buckner, R. L., Sepulcre, J., Talukdar, T., Krienen, F. M., Liu, H., Hedden, T., … Johnson, K. A. (2009). Cortical hubs revealed by intrinsic functional connectivity: Mapping, assessment of stability, and relation to Alzheimer's disease. *The Journal of Neuroscience: The Official Journal of the Society for Neuroscience*, *29*, 1860–1873.

Bullmore, E., & Sporns, O. (2009). Complex brain networks: Graph theoretical analysis of structural and functional systems. *Nature Reviews. Neuroscience*, *10*, 186–198.

Chang, C., & Glover, G. H. (2010). Time-frequency dynamics of resting-state brain connectivity measured with fMRI. *NeuroImage*, *50*, 81–98.

Chen, J. L., Ros, T., & Gruzelier, J. H. (2013). Dynamic changes of ICA-derived EEG functional connectivity in the resting state. *Human Brain Mapping*, *34*, 852–868.

Christoff, K., Irving, Z. C., Fox, K. C., Spreng, R. N., & Andrews-Hanna, J. R. (2016). Mind-wandering as spontaneous thought: A dynamic framework. *Nature Reviews. Neuroscience*, *17*, 718–731.

Coito, A., Genetti, M., Pittau, F., Iannotti, G. R., Thomschewski, A., Holler, Y., … Vulliemoz, S. (2016a). Altered directed functional connectivity in temporal lobe epilepsy in the absence of interictal spikes: A high density EEG study. *Epilepsia*, *57*, 402–411.

Coito, A., Michel, C. M., van Mierlo, P., Vulliemoz, S., & Plomp, G. (2016). Directed functional brain connectivity based on EEG source imaging: Methodology and application to temporal lobe epilepsy. *IEEE Transactions on Bio-Medical Engineering*, *63*, 2619–2628.

Coito, A., Plomp, G., Genetti, M., Abela, E., Wiest, R., Seeck, M., … Vulliemoz, S. (2015). Dynamic directed interictal connectivity in left and right temporal lobe epilepsy. *Epilepsia*, *56*, 207–217.

Cole, M. W., Pathak, S., & Schneider, W. (2010). Identifying the brain's most globally connected regions. *NeuroImage*, *49*, 3132–3148.

Corbetta, M., & Shulman, G. L. (2002). Control of goal-directed and stimulus-driven attention in the brain. *Nature Reviews. Neuroscience*, *3*, 201–215.

Damoiseaux, J. S., Rombouts, S. A., Barkhof, F., Scheltens, P., Stam, C. J., Smith, S. M., & Beckmann, C. F. (2006). Consistent resting-state networks across healthy subjects. *Proceedings of the National Academy of Sciences of the United States of America*, *103*, 13848–13853.

Darvas, F., Pantazis, D., Kucukaltun-Yildirim, E., & Leahy, R. M. (2004). Mapping human brain function with MEG and EEG: Methods and validation. *NeuroImage*, *23*(Suppl 1), S289–S299.

De Luca, M., Beckmann, C. F., De Stefano, N., Matthews, P. M., & Smith, S. M. (2006). fMRI resting state networks define distinct modes of long-distance interactions in the human brain. *NeuroImage*, *29*, 1359–1367.

de Pasquale, F., Della Penna, S., Snyder, A. Z., Lewis, C., Mantini, D., Marzetti, L., … Corbetta, M. (2010). Temporal dynamics of spontaneous MEG activity in brain networks. *Proceedings of the National Academy of Sciences of the United States of America*, *107*, 6040–6045.

Deshpande, G., Santhanam, P., & Hu, X. (2011). Instantaneous and causal connectivity in resting state brain networks derived from functional MRI data. *NeuroImage*, *54*, 1043–1052.

Di, X., & Biswal, B. B. (2014). Identifying the default mode network structure using dynamic causal modeling on resting-state functional magnetic resonance imaging. *NeuroImage*, *86*, 53–59.

Ding, L., Worrell, G. A., Lagerlund, T. D., & He, B. (2007). Ictal source analysis: Localization and imaging of causal interactions in humans. *NeuroImage*, *34*, 575–586.

Fransson, P., & Marrelec, G. (2008). The precuneus/posterior cingulate cortex plays a pivotal role in the default mode network: Evidence from a partial correlation network analysis. *NeuroImage*, *42*, 1178–1184.

Ghumare, E., Schrooten, M., Vandenberghe, R., & Dupont, P. (2015) *Comparison of different Kalman filter approaches in deriving time varying connectivity from EEG data*. Conference proceedings: … Annual International Conference of the IEEE Engineering in Medicine and Biology Society. IEEE Engineering in Medicine and Biology Society. Annual Conference, 2015, 2199–202.

Granger, C. W. J. (1969). Investigating causal relations by econometric models and cross-spectral methods. *Econometrica*, *37*, 424–438.

Grave de Peralta Menendez, R., Murray, M. M., Michel, C. M., Martuzzi, R., & Gonzalez Andino, S. L. (2004). Electrical neuroimaging based on biophysical constraints. *NeuroImage*, *21*, 527–539.

Greicius, M. (2008). Resting-state functional connectivity in neuropsychiatric disorders. *Current Opinion in Neurology*, *21*, 424–430.

Greicius, M. D., Krasnow, B., Reiss, A. L., & Menon, V. (2003). Functional connectivity in the resting brain: A network analysis of the default mode hypothesis. *Proceedings of the National Academy of Sciences of the United States of America*, *100*, 253–258.

Greicius, M. D., Srivastava, G., Reiss, A. L., & Menon, V. (2004). Default-mode network activity distinguishes Alzheimer's disease from healthy aging: Evidence from functional MRI. *Proceedings of the National Academy of Sciences of the United States of America*, *101*, 4637–4642.

Greicius, M. D., Supekar, K., Menon, V., & Dougherty, R. F. (2009). Resting-state functional connectivity reflects structural connectivity in the default mode network. *Cerebral Cortex*, *19*, 72–78.

Gusnard, D. A., & Raichle, M. E. (2001). Searching for a baseline: Functional imaging and the resting human brain. *Nature Reviews. Neuroscience*, *2*, 685–694.

Hagmann, P., Cammoun, L., Gigandet, X., Meuli, R., Honey, C. J., Wedeen, V. J., & Sporns, O. (2008). Mapping the structural core of human cerebral cortex. *PLoS Biology*, *6*, e159.

Hayden, B. Y., Smith, D. V., & Platt, M. L. (2009). Electrophysiological correlates of default-mode processing in macaque posterior cingulate cortex. *Proceedings of the National Academy of Sciences of the United States of America*, *106*, 5948–5953.

He, B., Dai, Y., Astolfi, L., Babiloni, F., Yuan, H., & Yang, L. (2011). eConnectome: A MATLAB toolbox for mapping and imaging of brain functional connectivity. *Journal of Neuroscience Methods*, *195*, 261–269.

Honey, C. J., Sporns, O., Cammoun, L., Gigandet, X., Thiran, J. P., Meuli, R., & Hagmann, P. (2009). Predicting human resting-state functional connectivity from structural connectivity. *Proceedings of the National Academy of Sciences of the United States of America*, *106*, 2035–2040.

Horn, A., Ostwald, D., Reisert, M., & Blankenburg, F. (2014). The structural-functional connectome and the default mode network of the human brain. *NeuroImage*, *102*(Pt 1), 142–151.

Jiao, Q., Lu, G., Zhang, Z., Zhong, Y., Wang, Z., Guo, Y., … Liu, Y. (2011). Granger causal influence predicts BOLD activity levels in the default mode network. *Human Brain Mapping*, *32*, 154–161.

Karahanoglu, F. I., & Van De Ville, D. (2015). Transient brain activity disentangles fMRI resting-state dynamics in terms of spatially and temporally overlapping networks. *Nature Communications*, *6*, 7751.

Koenig, T., & Pascual-Marqui, R. D. (2009). Multichannel frequency and time-frequency analysis. In C. M. Michel, T. Koenig, D. Brandeis, L. R. R. Gianotti, & J. Wackermann (Eds.), *Electrical neuroimaging: Cambridge Medicine*.

Koessler, L., Cecchin, T., Colnat-Coulbois, S., Vignal, J. P., Jonas, J., Vespignani, H., … Maillard, L. G. (2015). Catching the invisible: Mesial temporal source contribution to simultaneous EEG and SEEG recordings. *Brain Topography*, *28*, 5–20.

Kus, R., Kaminski, M., & Blinowska, K. J. (2004). Determination of EEG activity propagation: Pair-wise versus multichannel estimate. *IEEE Transactions on Bio-Medical Engineering*, *51*, 1501–1510.

Laufs, H., Krakow, K., Sterzer, P., Eger, E., Beyerle, A., Salek-Haddadi, A., & Kleinschmidt, A. (2003). Electroencephalographic signatures of attentional and cognitive default modes in spontaneous brain activity fluctuations at rest. *Proceedings of the National Academy of Sciences of the United States of America*, *100*, 11053–11058.

Li, B., Wang, X., Yao, S., Hu, D., & Friston, K. (2012). Task-dependent modulation of effective connectivity within the default mode network. *Frontiers in Psychology*, *3*, 206.

Liu, Q., Farahibozorg, S., Porcaro, C., Wenderoth, N., & Mantini, D. (2017). Detecting large-scale networks in the human brain using high-density electroencephalography. *Human Brain Mapping*, *38*, 4631–4643.

Lizier, J. T., Heinzle, J., Horstmann, A., Haynes, J. D., & Prokopenko, M. (2011). Multivariate information-theoretic measures reveal directed information structure and task relevant changes in fMRI connectivity. *Journal of Computational Neuroscience*, *30*, 85–107.

Lopes da Silva, F. (2013). EEG and MEG: Relevance to neuroscience. *Neuron*, *80*, 1112–1128.

Maldjian, J. A., Davenport, E. M., & Whitlow, C. T. (2014). Graph theoretical analysis of resting-state MEG data: Identifying interhemispheric connectivity and the default mode. *NeuroImage*, *96*, 88–94.

Mantini, D., Perrucci, M. G., Del Gratta, C., Romani, G. L., & Corbetta, M. (2007). Electrophysiological signatures of resting state networks in the human brain. *Proceedings of the National Academy of Sciences of the United States of America*, *104*, 13170–13175.

Marple, S. L. (1987). *Digital spectral analysis with applications*. Upper Saddle River, NJ: Prentice-Hall, Inc.

Megevand, P., Spinelli, L., Genetti, M., Brodbeck, V., Momjian, S., Schaller, K., … Seeck, M. (2014). Electric source imaging of interictal activity accurately localises the seizure onset zone. *Journal of Neurology, Neurosurgery, and Psychiatry*, *85*, 38–43.

Michalareas, G., Vezoli, J., van Pelt, S., Schoffelen, J. M., Kennedy, H., & Fries, P. (2016). Alpha-Beta and Gamma rhythms subserve feedback and feedforward influences among human visual cortical areas. *Neuron*, *89*, 384–397.

Michel, C. M., Lantz, G., Spinelli, L., De Peralta, R. G., Landis, T., & Seeck, M. (2004). 128-channel EEG source imaging in epilepsy: Clinical yield and localization precision. *Journal of Clinical Neurophysiology*, *21*, 71–83.

Nahum, L., Gabriel, D., Spinelli, L., Momjian, S., Seeck, M., Michel, C. M., & Schnider, A. (2011). Rapid consolidation and the human hippocampus: Intracranial recordings confirm surface EEG. *Hippocampus*, *21*, 689–693.

Pagnotta, M. F., & Plomp, G. (2018). Time-varying MVAR algorithms for directed connectivity analysis: Critical comparison in simulations and benchmark EEG data. *PLoS One*, *13*, e0198846.

Parvizi, J., Van Hoesen, G. W., Buckwalter, J., & Damasio, A. (2006). Neural connections of the posteromedial cortex in the macaque. *Proceedings of the National Academy of Sciences of the United States of America*, *103*, 1563–1568.

de Pasquale, F., Corbetta, M., Betti, V., Della Penna, S. (2017) Cortical cores in network dynamics. *NeuroImage*

Pfurtscheller, G., & Lopes da Silva, F. H. (1999). Event-related EEG/MEG synchronization and desynchronization: Basic principles. *Clinical Neurophysiology: Official Journal of the International Federation of Clinical Neurophysiology*, *110*, 1842–1857.

Plomp, G., Hervais-Adelman, A., Astolfi, L., & Michel, C. M. (2015). Early recurrence and ongoing parietal driving during elementary visual processing. *Scientific Reports*, *5*, 18733.

Plomp, G., Leeuwen, C., & Ioannides, A. A. (2010). Functional specialization and dynamic resource allocation in visual cortex. *Human Brain Mapping*, *31*, 1–13.

Plomp, G., Quairiaux, C., Michel, C. M., & Astolfi, L. (2014). The physiological plausibility of time-varying granger-causal modeling: Normalization and weighting by spectral power. *NeuroImage*, *97*, 206–216.

Raichle, M. E., MacLeod, A. M., Snyder, A. Z., Powers, W. J., Gusnard, D. A., & Shulman, G. L. (2001). A default mode of brain function. *Proceedings of the National Academy of Sciences of the United States of America*, *98*, 676–682.

Ramantani, G., Dumpelmann, M., Koessler, L., Brandt, A., Cosandier-Rimele, D., Zentner, J., … Maillard, L. G. (2014). Simultaneous subdural and scalp EEG correlates of frontal lobe epileptic sources. *Epilepsia*, *55*, 278–288.

Razi, A., Kahan, J., Rees, G., & Friston, K. J. (2015). Construct validation of a DCM for resting state fMRI. *NeuroImage*, *106*, 1–14.

Rikir, E., Koessler, L., Gavaret, M., Bartolomei, F., Colnat-Coulbois, S., Vignal, J. P., … Maillard, L. G. (2014). Electrical source imaging in cortical malformation-related epilepsy: A prospective EEG-SEEG concordance study. *Epilepsia*, *55*, 918–932.

Rubinov, M., & Sporns, O. (2010). Complex network measures of brain connectivity: Uses and interpretations. *NeuroImage*, *52*, 1059–1069.

Saalmann, Y. B., Pinsk, M. A., Wang, L., Li, X., & Kastner, S. (2012). The pulvinar regulates information transmission between cortical areas based on attention demands. *Science*, *337*, 753–756.

Schlögl, A. (2006). A comparison of multivariate autoregressive estimators. *Signal Processing*, *86*, 2426–2429.

Schoffelen, J. M., & Gross, J. (2009). Source connectivity analysis with MEG and EEG. *Human Brain Mapping*, *30*, 1857–1865.

Sperdin, H. F., Coito, A., Kojovic, N., Rihs, T. A., Jan, R. K., Franchini, M., … Schaer, M. (2018). Early alterations of social brain networks in young children with autism. *eLife*, *7*.

Theiler, J., Eubank, S., Longtin, A., Galdrikian, B., & Doyne Farmer, J. (1992). Testing for nonlinearity in time series: The method of surrogate data. *Physica D*, *58*, 77–94.

Thut, G., Schyns, P. G., & Gross, J. (2011). Entrainment of perceptually relevant brain oscillations by non-invasive rhythmic stimulation of the human brain. *Frontiers in Psychology*, *2*, 170.

Tzourio-Mazoyer, N., Landeau, B., Papathanassiou, D., Crivello, F., Etard, O., Delcroix, N., … Joliot, M. (2002). Automated anatomical labeling of activations in SPM using a macroscopic anatomical parcellation of the MNI MRI single-subject brain. *NeuroImage*, *15*, 273–289.

Uddin, L. Q., Kelly, A. M., Biswal, B. B., Castellanos, F. X., & Milham, M. P. (2009). Functional connectivity of default mode network components: Correlation, anticorrelation, and causality. *Human Brain Mapping*, *30*, 625–637.

Van de Steen, F., Faes, L., Karahan, E., Songsiri, J., Valdes-Sosa, P. A., & Marinazzo, D. (2016). Critical comments on EEG sensor space dynamical connectivity analysis. *Brain topography*.

van den Heuvel, M., Mandl, R., Luigjes, J., & Hulshoff Pol, H. (2008). Microstructural organization of the cingulum tract and the level of default mode functional connectivity. *The Journal of Neuroscience: The Official Journal of the Society for Neuroscience*, *28*, 10844–10851.

van den Heuvel, M. P., Kahn, R. S., Goni, J., & Sporns, O. (2012). High-cost, high-capacity backbone for global brain communication. *Proceedings of the National Academy of Sciences of the United States of America*, *109*, 11372–11377.

van Oort, E.S., van Cappellen van Walsum, A.M., Norris, D.G. (2014) An investigation into the functional and structural connectivity of the default mode network, *NeuroImage*, *90*:381–9.

Vidaurre, D., Quinn, A. J., Baker, A. P., Dupret, D., Tejero-Cantero, A., & Woolrich, M. W. (2016). Spectrally resolved fast transient brain states in electrophysiological data. *NeuroImage*, *126*, 81–95.

Vogt, B. A., & Laureys, S. (2005). Posterior cingulate, precuneal and retrosplenial cortices: Cytology and components of the neural network correlates of consciousness. *Progress in Brain Research*, *150*, 205–217.

Yan, C., & He, Y. (2011). Driving and driven architectures of directed small-world human brain functional networks. *PLoS One*, *6*, e23460.

Yuan, H., Doud, A., Gururajan, A., & He, B. (2008). Cortical imaging of event-related (de) synchronization during online control of brain-computer interface using minimum-norm estimates in frequency domain. *IEEE Transactions on Neural Systems and Rehabilitation Engineering: A Publication of the IEEE Engineering in Medicine and Biology Society*, *16*, 425–431.

Zalesky, A., Fornito, A., Cocchi, L., Gollo, L. L., & Breakspear, M. (2014). Time-resolved resting-state brain networks. *Proceedings of the National Academy of Sciences of the United States of America*, *111*, 10341–10346.

Zhou, Z., Wang, X., Klahr, N. J., Liu, W., Arias, D., Liu, H., … Liu, Y. (2011). A conditional granger causality model approach for group analysis in functional magnetic resonance imaging. *Magnetic Resonance Imaging*, *29*, 418–433.

SUPPORTING INFORMATION

Additional supporting information may be found online in the Supporting Information section at the end of the article.

How to cite this article: Coito A, Michel CM, Vulliemoz S, Plomp G. Directed functional connections underlying spontaneous brain activity. *Hum Brain Mapp*. 2019;40:879–888. https://doi.org/10.1002/hbm.24418